Chinese Chemical Letters 33 (2022) 3556–3560

Contents lists available at ScienceDirect

Chinese Chemical Letters

journal homepage: www.elsevier.com/locate/cclet

Efficient gaseous iodine capture enhanced by charge-induced effect of covalent organic frameworks with dense tertiary-amine nodes

Bo Jiang[1], Yue Qi[1], Xiaofeng Li, Xinghua Guo, Zhimin Jia, Jie Zhang, Yang Li*, Lijian Ma*

College of Chemistry, Sichuan University, Chengdu 610064, China

ARTICLE INFO

Article history:
Received 5 January 2022
Revised 10 March 2022
Accepted 14 March 2022
Available online 16 March 2022

Keywords:
Covalent organic frameworks
Tertiary-amine nodes
Charge-induced effect
Gaseous iodine capture
DFT theoretical calculation

ABSTRACT

Based on the outstanding application advantages of nitrogen-rich materials with regular porous frameworks in the capture of gaseous radioactive iodine, a series of covalent organic frameworks (COFs) with dual channels and abundant tertiary-amine active sites were constructed herein *via* a unique multi-nitrogen node design. The high density of up-to-six nitrogen adsorption sites in a single structural unit of the products effectively improved the adsorption capacities of the materials for iodine. Moreover, the adsorption affinity of the active sites can be further regulated by charge-induced effect of different electron-donating groups introduced into the COFs. Adsorption experiments combined with DFT theoretical calculations confirmed that the introduction of electron-donating groups can effectively increase the electron density around the active sites and enhance the binding energy between the materials and iodine, and thus improve the iodine adsorption capacity to 5.54 g/g. The construction strategy of multi-nitrogen node and charge-induced effect proposed in this study provides an important guidance for the study of the structure-activity relationship of functional materials and the design and preparation of high-performance iodine adsorption materials.

As an important gaseous fission product produced by nuclear reactors, radioactive iodine is one of the major hazardous vapor radioactive pollutants released during nuclear power plant operation, spent fuel reprocessing and nuclear accidents. Due to its strong volatility, high diffusion coefficient and long half-life, *etc.*, it is quite difficult to deal with in the actual environment. For example, the half-life of ^{129}I is up to 1.57×10^7 years, which can easily cause serious harm to human health and the environment. Although ^{131}I has a short half-life of 8.02 days, it also plays a vital role in causing radiation hazard to human beings in a short term, such as being easy to accumulate and induce diseases in the thyroid, owing to its high specific activity, biocompatibility and chemical toxicity. Therefore, rapid and efficient separation and enrichment of radioactive iodine is of great practical significance [1].

In recent years, researchers have made great efforts in the study of efficient capture and storage materials for radioactive iodine, including activated carbon [2], conjugated microporous polymers [3–5], metal-organic frameworks [6–8], porous organic polymers [9,10], *etc.* However, these iodine adsorbents have some defects such as poor structural stability, few active sites and low adsorption capacity to some extent, which limit their application in gaseous iodine removal in actual extreme environment.

The emerging covalent organic frameworks (COFs) are regarded as one of the most promising adsorption materials due to their periodic structure, regular pores, large specific surface area and high porosity. COFs have shown exciting enrichment and separation effects on vapor iodine in some researches [11–14]. Although great progress has been made so far, designing and synthesizing high-capacity COFs for iodine capture is still a huge challenge. Previous studies have shown that electron-rich structural units in materials can effectively form charge transfer complexes with electron-deficient iodine molecule, thereby improving the iodine capture performance of the materials [1,15]. Especially, materials with nitrogen-rich structure have obvious advantages for iodine capture. For example, the introduction of structural units such as amine, imine, triazine ring, pyridine and imidazole into the structural system can significantly increase the adsorption capacity of the COFs for iodine [12,16–18]. However, most imine-linked COFs commonly designed and studied at present have fewer chemical active sites. On the other hand, the triazine ring units usually used for the introduction of nitrogen-rich structure will generally reduce the affinity between their active sites (C=N groups) and iodine,

* Corresponding authors.
E-mail addresses: ly7701850@163.com (Y. Li), ma.lj@hotmail.com (L. Ma).
[1] These authors contributed equally to this work.

https://doi.org/10.1016/j.cclet.2022.03.053
1001-8417/

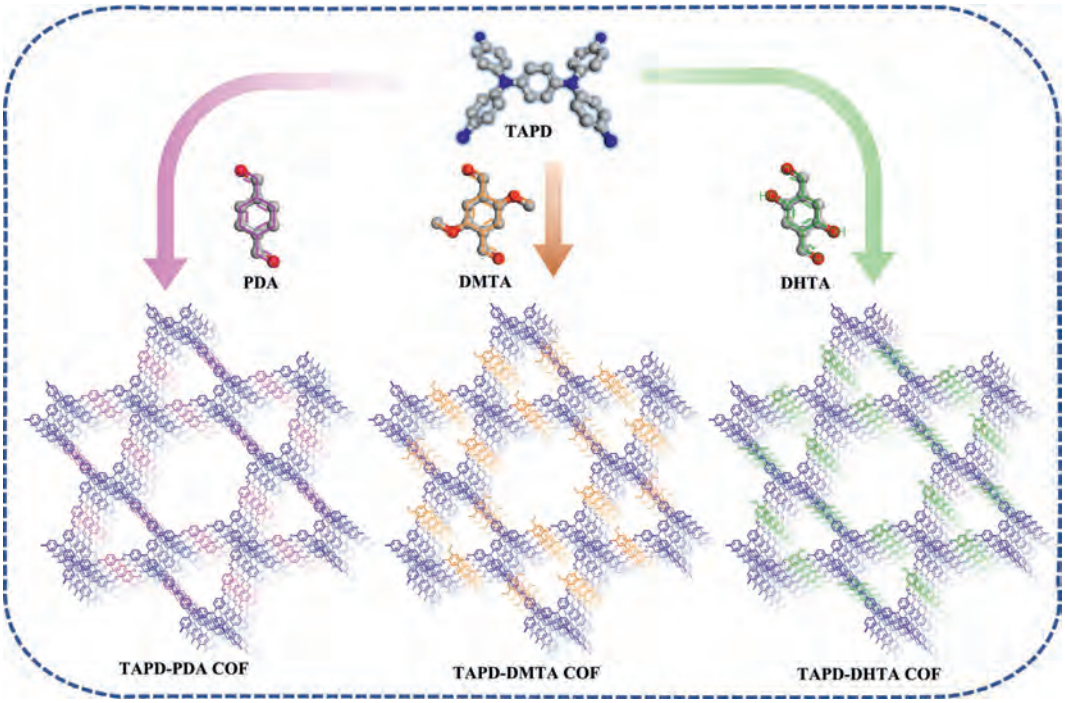

Scheme 1. Schematic diagram of the COF syntheses (gray, C; blue, N; red, O).

owing to the formation of large conjugated systems by the triazine rings.

Based on the above theory, how to construct materials with regular channels and improve the density of adsorption sites on the materials, and meanwhile effectively ensure the high activity and efficiency of these adsorption sites as well as the high affinity for iodine has become the key to prepare high-performance iodine capture materials. In order to achieve this goal, a series of 2D COFs with hexagonal and triangular pore characteristics were designed and constructed from a spatially twisted four-link multi-nitrogen nodes building block (tetrakis(4-aminophenyl)−1,4-benzenediamine (TAPD)). Each structural unit has up to 6 effective nitrogen binding sites, including the nitrogen of tertiary amine with high adsorption activity. The high-density of active adsorption sites can fully guarantee the materials' iodine adsorption capacity, and the spatial distortion of the structure can effectively improve the permeability of the pore, and thus improve the materials' iodine adsorption rate. In addition, different electron-donating groups are also introduced into COFs to further enhance the adsorption affinity of the active sites for iodine. The charge-induced effect of the electron-donating groups also greatly improved the iodine adsorption performance of the materials. The strategy of multi-nitrogen node and charge-induced effect proposed for the first time in this study for COF construction has significant scientific value for the in-depth study of the structure and properties of COFs as well as the preparation of high-performance iodine adsorbents.

In this study, TAPD-PDA COF, TAPD-DMTA COF and TAPD-DHTA COF were synthesized by the polycondensation of TAPD with terephthalaldehyde (PDA), 2,5-dimethoxyterephthalaldehyde (DMTA) and 2,5-dihydroxyterephthalaldehyde (DHTA), respectively under solvothermal conditions (Scheme 1, details in Supporting information) [19,20]. The Fourier transform infrared (FT-IR) spectra of the products showed that the characteristic peaks of C=O in the range of 1664–1686 cm^{-1} and -NH_2 in the range of 3346–3430 cm^{-1} almost disappeared, and the stretching vibration peak of C=N (1610–1620 cm^{-1}) appeared, indicating the successful occurrence of aldehyde-amine condensation reaction (Figs. S1a–c in Supporting information). The elemental contents of the prepared COFs determined by elemental analysis indicated that the experimental values of C/H/N are close to the theoretical values (Table S1 in Supporting information). The results of thermogravimetric analysis (TGA) showed that all the COFs have high thermal stability (Fig. S2a in Supporting information). The X-ray photoelectron spectroscopy (XPS) analysis revealed that there are nitrogen peaks of tertiary amine and imine in the N1s spectrum with a ratio of 1:2 (Fig. S3 in Supporting information). Scanning electron microscopy (SEM) was used to characterize the micromorphology of the COFs and the nanosheet-like layered structures can be obviously seen in the SEM images (Fig. S4 in Supporting information).

As can be seen from the powder X-ray diffraction (PXRD) patterns (Figs. 1a–c), TAPD-PDA COF, TAPD-DMTA COF and TAPD-DHTA COF all have high crystallinity and have a strong diffraction peak belonging to (100) crystal plane at about 2.35° Materials Studio 8.0 software was used to simulate and analyze the material structure. It was found that the experimental PXRD patterns of the three COFs are consistent with the simulated patterns of eclipsed (AA) stacking mode. The fine structural images (Fig. 1d and Fig. S5 in Supporting information) obtained by high-resolution transmission electron microscopy (HR-TEM) proved that the materials have good crystal structure. The specific surface areas and pore structure of the materials were studied by nitrogen adsorption isotherm at 77 K, and the measured Brunauer–Emmett–Teller (BET) surface areas of TAPD-PDA COF, TAPD-DMTA COF and TAPD-DHTA COF are 194.1, 415.2 and 213.6 m^2/g, respectively. The pore size distributions analyzed by non-local density functional theory (NLDFT) showed that all the materials have two different pore sizes and their average pore sizes are about ~1.81/2.78 nm, ~1.23/2.60 nm, ~1.56/2.73 nm, respectively, which are basically consistent with the simulated pore sizes (Fig. S6 in Supporting information). The results further proved that the three COFs are AA stacking mode and Kagome (kgm) topological configuration with two different pore channels.

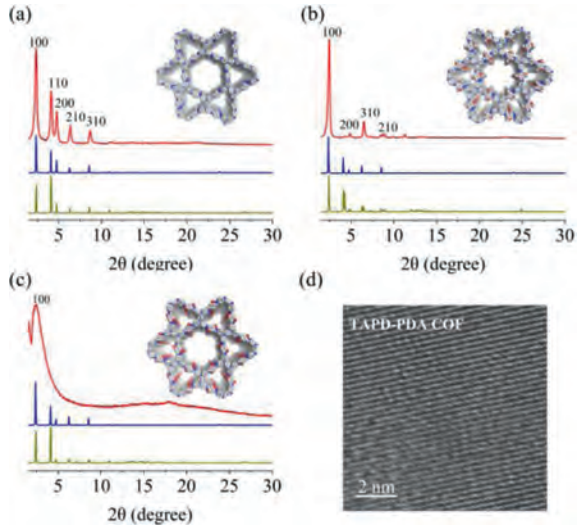

Fig. 1. Experimental (red), AA stacking (blue) and AB stacking (green) simulation PXRD patterns of TAPD-PDA COF (a), TAPD-DMTA COF (b) and TAPD-DHTA COF (c) (inset: the views of space-filling models of AA stacking); HR-TEM image of TAPD-PDA COF (d).

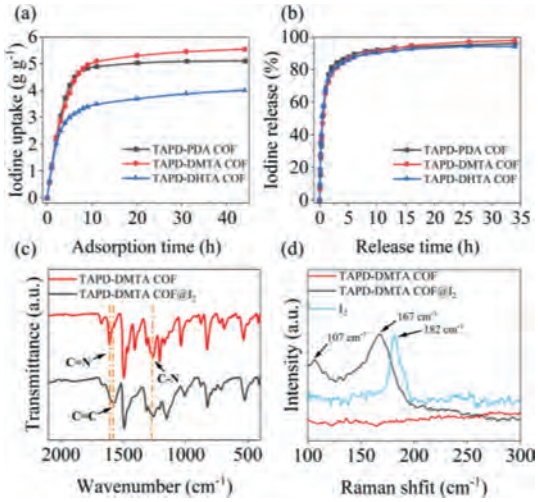

Fig. 2. Gravimetric iodine uptake at 75 °C and ambient pressure (a) and iodine release at 125 °C (b) of TAPD-PDA COF (black), TAPD-DMTA COF (red) and TAPD-DHTA COF (blue); FT-IR spectra (c) and Raman spectra (d) of TAPD-DMTA COF before and after iodine uptake.

In view of the high specific surface areas and the periodic distribution of double channels, as well as the abundant nitrogen active sites of the COFs, their adsorption properties for gaseous iodine were investigated. The iodine-loaded materials after the adsorption were named TAPD-PDA COF@I_2, TAPD-DMTA COF@I_2 and TAPD-DHTA COF@I_2 (Fig. 2a). It was found that the adsorption capacities of the materials increased rapidly in the initial 6 h and reached the maximum values after ~44 h (Table S2 in Supporting information). The maximum adsorption capacities of TAPD-PDA COF, TAPD-DMTA COF and TAPD-DHTA COF are 5.09, 5.54 and 4.02 g/g, respectively, indicating that the construction strategy of multi-nitrogen nodes is effective for preparing high-performance iodine adsorbents.

The desorption experiments revealed that TAPD-PDA COF@I_2, TAPD-DMTA COF@I_2 and TAPD-DHTA COF@I_2 have faster iodine release rates and more than 80% of the adsorbed iodine can be released within 3 h at 125 °C (Fig. 2b and Table S3 in Supporting information). In addition, TGA was used to study the heat release of iodine in TAPD-DMTA COF@I_2 under N_2 atmosphere (Fig. S2b in Supporting information). Extensive mass loss was observed between 25 °C and 350 °C, mainly due to the release of iodine captured by the materials. The amount of iodine released at 350 °C reached 85.6% of the weight of TAPD-DMTA COF@I_2, which was basically the same as the amount of iodine captured by TAPD-DMTA COF (84.7%).

The iodine capture mechanism of the materials was preliminarily studied by FT-IR and Raman spectra. As seen from the FT-IR spectra in Fig. 2c, the characteristic peaks changed significantly before and after adsorption. For example, the stretching vibration peak of C=N at 1612 cm^{-1} disappeared obviously after the iodine adsorption, and the peak of C=C (1577 cm^{-1}) in phenyl ring was significantly enhanced. Meanwhile, the stretching vibration peak of C–N in the tertiary amine node at 1261 cm^{-1} became weak and shifted to 1255 cm^{-1} [21,22]. The results indicated that the iodine adsorption had occurred simultaneously in imine and tertiary amine groups of TAPD-DMTA COF. The species of the adsorbed iodine was detected by Raman spectra in Fig. 2d. Compared with the original COFs, TAPD-DMTA COF@I_2 has strong absorption peaks at 107 and 167 cm^{-1}, which are assigned to the aggregated state I_3^- and I_5^-, respectively, and there is no characteristic peak of I_2, indicating that the iodine molecules are basically converted into poly-anion iodides [14,23]. The consistency of the Raman and FT-IR spectra indicated that the occurrence of chemical adsorption process, which was due to the charge transfer between the electron-rich imine bond and the electron-deficient iodine molecule, forming a stable charge transfer complex (Scheme 2) [15].

In order to further explore the mechanism of iodine adsorption by the COFs and reveal the internal driving force of the difference in adsorption capacity, density functional theory (DFT) was carried out to simulate and calculate the adsorption process. As shown in Fig. 3, TAPD-PDA, TAPD-DMTA and TAPD-DHTA were used as model molecules to represent TAPD-PDA COF, TAPD-DMTA COF and TAPD-DHTA COF, respectively. Iodine molecules were adsorbed at two different active sites of tertiary amine nitrogen and imine nitrogen. The calculated binding energy between iodine and TAPD-DMTA is −17.32 kcal/mol, which is lower than that of TAPD-PDA (−15.95 kcal/mol) and TAPD-DHTA (−14.91 kcal/mol), indicating that TAPD-DMTA has a stronger affinity for iodine, while TAPD-DHTA has the worst affinity for iodine. This conclusion is also consistent with the experimental results of saturated iodine adsorption (TAPD-DMTA COF > TAPD-PDA COF > TAPD-DHTA COF). Based on the calculations, it can be concluded that the introduction of methoxy, an electron-donating group, into the structure can increase the electron cloud density around the nitrogen active site through the charge-induced effect, thereby enhancing the affinity of the active site for iodine. On the other hand, although the introduced hydroxyl group can also be regarded as an electron-donating group, it is more inclined to form intramolecular hydrogen bond with the nitrogen in the *ortho*-imine bond, which reduces the electron cloud density near the nitrogen active site and lead to a worse affinity for iodine finally [24–26]. Moreover, ESP analysis was also performed on 0.001 a.u. contours of electronic density for the three systems [27–30]. From the van der Waals (vdW) surface penetration diagram, negative ESP (blue area) is mainly distributed on the vdW surface of the model molecules and delocalized around tertiary amines, imines and phenyl rings, while the vdW surface of iodine is mainly positive ESP (red area) and the mutual penetration between red and blue indicates the interaction between them. Obviously from the ESP diagram, it can be found that compared to TAPD-PDA, the negative ESP of TAPD-DMTA is more delocalized around tertiary amines, imines and phenyl rings, while TAPD-DHPA even exhibits a positive ESP near tertiary amines and imines. The ESP analysis results agree well with DFT calcula-

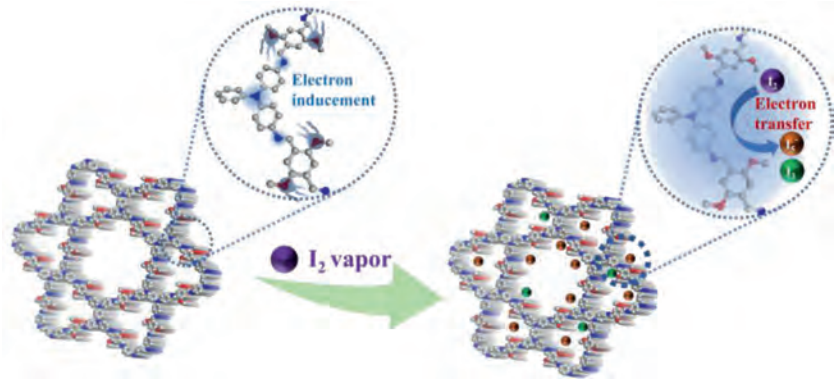

Scheme 2. Schematic illustration of the iodine uptake mechanism of TAPD-DMTA COF (gray, C; blue, N; red, O; purple, I_2; green, I_3^-; brown, I_5^-).

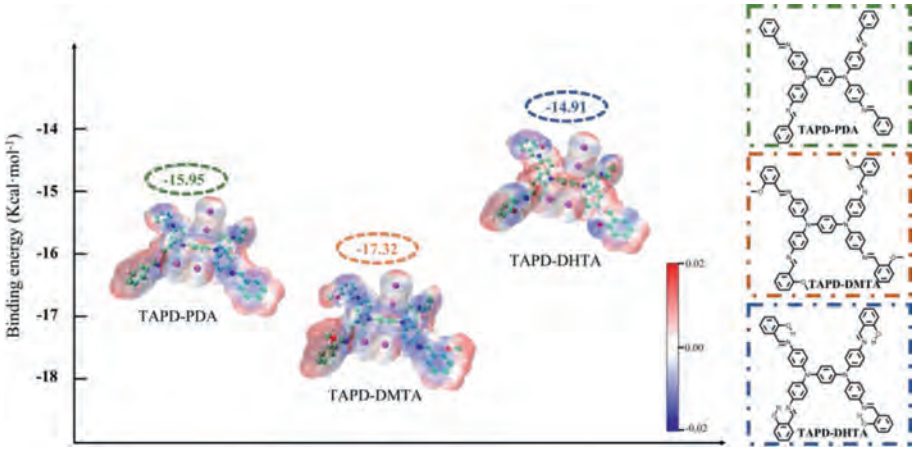

Fig. 3. Structural formulas of TAPD-PDA, TAPD-DMTA and TAPD-DHTA (right) and the binding energy with iodine and ESP analysis (left) (green, C; white, H; red, O; blue, N; purple, I).

tions and experimental conclusions, which can fully explain the internal mechanism of the difference in iodine adsorption performance of TAPD-PDA COF, TAPD-DMTA COF and TAPD-DHTA COF.

In summary, based on the affinity of the nitrogen-rich and electron-rich structure for vapor iodine adsorption, we designed and constructed a series of 2D COFs with double channels and abundant active adsorption sites of tertiary nitrogen using a unique multi-nitrogen node TAPD, and further enhanced the adsorption affinity of active sites to iodine by introducing different electron-donating groups to regulate the charge-induced effect in the structural frameworks. Adsorption experiments combined with DFT theoretical calculations show that the introduced methoxyl group can effectively improve the electron density around the active sites, thereby enhance the binding energy between the material and iodine and thus achieve a higher iodine adsorption capacity of 5.54 g/g. However, hydroxyl groups introduced into the structure tend to form intramolecular hydrogen bonds with nitrogens of the ortho-imine bonds, which induces a decrease in the electron density around the active sites and leads to a lower iodine adsorption capacity finally. This work not only prepares iodine adsorbents with high capacities using a construction strategy of multi-nitrogen node, but also confirms the effect of charge-induced groups on iodine adsorption through the combination of theory and experiments, which provides a valuable guiding strategy for in-depth research on the structure-activity relationship of functional materials and the design and preparation of high-performance materials for iodine adsorption.

Declaration of competing interest

The authors declare that they have no known competing financial interests or personal relationships that could have appeared to influence the work reported in this paper.

Acknowledgments

This work was supported by the National Natural Science Foundation of China (No. 21976125) and the Sichuan Science and Technology Program (Nos. 2020JDRC0014 and 2021YFG0229). We would like to thank the Analytical & Testing Center of Sichuan University for providing Materials studio and we would be grateful to Daichuan Ma and Daibing Luo for their help of computational simulation. We thank Shiyanjia Lab (www.shiyanjia.com) for the HR-TEM analysis. We are also grateful for the support from the Fundamental Research Funds for the Central Universities and the Comprehensive Training Platform Specialized Laboratory, College of chemistry, Sichuan University.

Supplementary materials

Supplementary material associated with this article can be found, in the online version, at doi:10.1016/j.cclet.2022.03.053.

References

[1] W. Xie, D. Cui, S.R. Zhang, Y.H. Xu, D.L. Jiang, Mater. Horiz. 6 (2019) 1571–1595.

[2] T.C.T. Pham, S. Docao, I.C. Hwang, et al., Energy Environ. Sci. 9 (2016) 1050–1062.
[3] A. Sigen, Y. Zhang, Z. Li, et al., Chem. Commun. 50 (2014) 8495–8498.
[4] X. Qian, Z.Q. Zhu, et al., ACS Appl. Mater. Interfaces 8 (2016) 21063–21069.
[5] T. Geng, C. Zhang, G. Chen, et al., Microporous Mesoporous Mater. 284 (2019) 468–475.
[6] D.F. Sava, M.A. Rodriguez, K.W. Chapman, et al., J. Am. Chem. Soc. 133 (2011) 12398–12401.
[7] D.F. Sava, K.W. Chapman, M.A. Rodriguez, et al., Chem. Mater. 25 (2013) 2591–2596.
[8] Y.Q. Hu, M.Q. Li, Y. Wang, et al., Chem. Eur. J. 23 (2017) 8409–8413.
[9] L. Liu, C. Song, A. Kong, Mater. Lett. 277 (2020) 128291.
[10] T.M. Geng, C. Hu, M. Liu, H.Y. Xia, Spectrochim. Acta Part A 258 (2021) 119852.
[11] Z.J. Yin, S.Q. Xu, T.G. Zhan, et al., Chem. Commun. 53 (2017) 7266–7269.
[12] C. Wang, Y. Wang, R. Ge, et al., Chem. Eur. J. 24 (2018) 585–589.
[13] X. Guo, Y. Li, M. Zhang, et al., Angew. Chem. Int. Ed. 59 (2020) 22697–22705.
[14] J. Li, H. Zhang, L. Zhang, et al., J. Mater. Chem. A 8 (2020) 9523–9527.
[15] J.T. Hughes, D.F. Sava, T.M. Nenoff, A. Navrotsky, J. Am. Chem. Soc. 135 (2013) 16256–16259.
[16] Y. Li, W. Chen, W. Hao, Y. Li, L. Chen, ACS. Appl. Nano Mater 1 (2018) 4756–4761.
[17] R. Chen, T. Hu, W. Zhang, C. He, Y. Li, Microporous Mesoporous Mater. 312 (2021) 110739.
[18] L. He, L. Chen, X. Dong, et al., Chem 7 (2021) 699–714.
[19] C. Krishnaraj, H. Sekhar Jena, L. Bourda, et al., J. Am. Chem. Soc. 142 (2020) 20107–20116.
[20] Q. Hao, Z.J. Li, B. Bai, et al., Angew. Chem. Int. Ed. 60 (2021) 12498–12503.
[21] Y. Li, X. Li, J. Li, et al., Microporous Mesoporous Mater. 325 (2021) 111351.
[22] I. Reva, L. Lapinski, N. Chattopadhyay, R. Fausto, Phys. Chem. Chem. Phys. 5 (2003) 3844–3850.
[23] Y. Lin, X. Jiang, S.T. Kim, et al., J. Am. Chem. Soc. 139 (2017) 7172–7175.
[24] X. Guo, Y. Tian, M. Zhang, et al., Chem. Mater. 30 (2018) 2299–2308.
[25] T. Lu, F. Chen, J. Comput. Chem. 33 (2012) 580–592.
[26] G. Das, T. Skorjanc, S.K. Sharma, et al., J. Am. Chem. Soc. 139 (2017) 9558–9565.
[27] L. Zhang, J. Li, H. Zhang, et al., Chem. Commun. 57 (2021) 5558–5561.
[28] A.D.William Humphrey, Klaus Schulten, J. Mol. Graph. 14 (1996) 33–38.
[29] J. Zhang, T. Lu, Phys. Chem. Chem. Phys. 23 (2021) 20323–20328.
[30] T. Lu, S. Manzetti, Struct. Chem. 25 (2014) 1521–1533.